1998

The observability of metal lines associated with the Ly alpha forest

U Hellsten

L Hernquist

N Katz
University of Massachusetts - Amherst

DH Weinberg

arXiv:astro-ph/9708090v2 19 Dec 1997

The Observability of Metal Lines Associated with the Lyman-alpha Forest

Uffe Hellsten and Lars Hernquist[1]
University of California, Lick Observatory, Santa Cruz, CA 95064

Neal Katz
University of Massachusetts, Dept. of Physics and Astronomy, Amherst, MA, 01003

and

David H. Weinberg
Ohio State University, Department of Astronomy, Columbus, OH 43210

ABSTRACT

We develop a prescription for characterizing the strengths of metal lines associated with Lyα forest absorbers (LYFAs) of a given neutral hydrogen column density $N_{\rm HI}$ and metallicity [O/H]. This *Line Observability Index* (LOX) is line-specific and translates, for weak lines, into a measure of the equivalent width. It can be evaluated quickly for thousands of transitions within the framework of a given model of the Lyα forest, providing a ranking of the absorption lines in terms of their strengths and enabling model builders to select the lines that deserve more detailed consideration, i.e. those that should be detectable in observed spectra of a given resolution and signal-to-noise ratio. We compute the LOX for a large number of elements and transitions in two cosmological models of the Lyα forest at $z \sim 3$ derived from hydrodynamic simulations of structure formation. We present results for a cold dark matter universe with a cosmological constant; an $\Omega = 1$ cold dark matter model yields nearly identical results, and we argue more generally that the LOX predictions are insensitive to the specific choice of cosmology. We also discuss how the LOX depends on redshift and on model parameters such as the mean baryonic density and radiation field.

We find that the OVI (1032 Å, 1038 Å) doublet is the best probe of the metallicity in low column density LYFAs ($N_{\rm HI} \approx 10^{14.5}{\rm cm}^{-2}$). Metallicities down to [O/H] $\sim$ -3 yield OVI absorption features that should be detectable in current high-quality spectra, provided that the expected position of the OVI feature is not contaminated by HI absorption. The strongest transitions in lower ionization states of oxygen are OV(630 Å), OIV(788 Å), and OIII(833 Å). These absorption lines are all predicted to be stronger than the OVI feature, but even at redshifts $3-4$ they will have to be observed in the ultraviolet, and they are extremely difficult to detect with present UV instruments, such as the Space Telescope Imaging Spectrograph (STIS). At lower

[1]Presidential Faculty Fellow

redshifts, detection of these lines may be possible in STIS spectra of the very brightest QSOs, while one may have to wait for next-generation instruments such as the Cosmic Origins Spectrograph (COS) to detect such lines in a number of high-redshift QSOs.

The strongest metal lines with restframe wavelength larger than 912Å associated with higher column density LYFAs at $z \sim 3$ are CIII (977 Å) and SiIII (1206.5 Å), which peak at $N_{\rm HI} \sim 10^{17}{\rm cm}^{-2}$. Of the lines with rest wavelengths $\lambda_r > 1216$Å, which can potentially be observed redwards of the Lyα forest, the CIV(1548,1551) doublet is expected to dominate in all LYFAs, regardless of the value of $N_{\rm HI}$. We argue that CIV and CII absorption may peak in different spatial regions, and that comparison of single-phase models of the CIV/CII ionization ratios with observed CIV/CII column density ratios can lead to an overestimate of the ionization parameter in the central parts of the absorbers.

Subject headings: Intergalactic medium: ionization, quasars: absorption lines

1. Introduction

Over the past decade, observations have demonstrated that strong Lyα forest absorbers (LYFAs) generally show associated metal line absorption (Meyer & York 1987; Lu 1991; Cowie et al. 1995; Womble et al. 1995; Songaila & Cowie 1996, hereafter SC). SC find CIV absorption in nearly all LYFAs at $z \sim 3$ with neutral column densities $N_{\rm HI} \gtrsim 1.6 \times 10^{15}\,{\rm cm}^{-2}$ and in $\simeq 75\%$ of systems with $N_{\rm HI} \gtrsim 3.2 \times 10^{14}$. The observed CIV column densities are consistent with the absorbers having a mean metallicity [C/H] ~ -2.5 and an intrinsic scatter in metallicity of about an order of magnitude (Rauch et al. 1996; Hellsten et al. 1997). An important question is whether or not a chemically pristine or extremely metal poor population of LYFAs exists, and if so, what the characteristic HI column densities of this population are. For $\log N_{\rm HI} \lesssim 14.5$ the associated CIV lines are close to the detection limits of SC, and it cannot yet be determined if these absorbers have the same metallicity distribution as those with higher $N_{\rm HI}$. Some theoretical models of early metal enrichment predict that the mean metallicity declines steadily with decreasing $N_{\rm HI}$ (Gnedin & Ostriker 1997).

Considerable progress has been made in the theoretical understanding of LYFAs. From the work of several groups (e.g. Cen et al. 1994; Zhang et al. 1995; Petitjean et al. 1995; Hernquist et al. 1996; Bi & Davidsen 1997) a picture has emerged in which the LYFAs are interpreted in terms of "Gunn-Peterson" absorption in an inhomogenous IGM pervaded by a background ionizing radiation field, presumed to originate from QSOs and perhaps young, star-forming galaxies. This picture links the Lyα forest directly to cosmological structure formation. The analysis of cosmological models of the LYFAs consists of producing artificial spectra by evaluating the absorption properties of the baryonic IGM along lines of sight through N-body and hydrodynamical simulations of structure formation. These spectra can then be analyzed in much the same way as observed QSO spectra, and the resulting distribution functions in $N_{\rm HI}$ and linewidths are found to agree quantitatively with those observed, lending considerable support to the cosmological LYFA picture (e.g. Miralda-Escudé et al. 1996; Davé et al. 1997; Zhang et al. 1997).

The interpretation of the metal line data within the framework of these models provides a strong test of this picture. If a metal enrichment pattern of the baryonic IGM is specified, the properties of selected absorption lines are readily calculated from the knowledge of densities, temperatures, and UV radiation field along the lines of sight (Haehnelt et al. 1996; Rauch et al. 1996; Hellsten et al. 1997). Until now, the metal lines considered have been limited to OVI(1032,1038), NV(1239,1243), CIV(1548,1551), SiIV(1394,1403), and CII(1335). These lines have been chosen because they have already been identified with LYFAs in real QSO spectra. With the exception of the OVI doublet they all have rest wavelengths $\lambda_0 > 1216$ Å, which means that for LYFAs at sufficiently high redshifts, they appear redward of the Lyα forest and hence are relatively easy to detect. Instead of making an a priori selection of a few metal lines to include in a cosmological model for LYFAs, a more satisfactory approach would be to make the models *predict* which metal lines, out of thousands of candidates, should be observable (in spectra of a given resolution and S/N) in LYFAs of different column densities. Such an approach would allow a comprehensive and swift selection of lines that deserve a more detailed treatment, depending on the specific purpose of the modeling. It would provide a sharper test of the model and place more stringent constraints on the metallicities and UV radiation spectrum, by making it possible to compare the complete list of metal lines predicted to be observable to the list of lines actually detected in QSO spectra, as well as the observed relative strengths of these lines.

This paper presents and applies a technique for implementing this comprehensive, a priori approach to metal line absorption predictions in cosmological models. In Section 2 we define a line observability index, which can easily be evaluated for a database of metal lines, within a particular model for LYFAs. This index is a measure of column density and hence allows the lines to be sorted by strength. It also predicts which lines should be detectable in LYFAs for a wide range of column densities and metallicities. In Section 3 we apply this technique to two specific cosmological models of the Lyα forest, based on hydrodynamic simulations of structure formation. In Section 4 we discuss the dependence of the LOX on model parameters such as the mean baryon density and radiation field and estimate how it changes with redshift, and we argue that the LOX has only a very weak dependence on the underlying cosmology. We discuss the results and summarize the conclusions in Section 5.

2. The Line Observability Index

Detection limits for absorption lines can be conveniently expressed in terms of the equivalent width

$$W_\lambda \equiv \int_0^\infty \left(1 - \frac{F_\lambda}{F_{c\lambda}}\right) d\lambda, \tag{1}$$

where $F_\lambda/F_{c\lambda}$ denotes the received energy flux per wavelength interval, normalized to the continuum level. For absorption lines that are weak enough to be optically thin, the rest frame equivalent width $W_{\lambda r}$ is proportional to the column density N of absorbing atoms along the line of sight

$$W_{\lambda r} = \frac{\pi\, e^2}{m_e c^2}\, N\, {\lambda_r}^2\, f, \tag{2}$$

where f and λ_r are the oscillator strength and rest frame wavelength of the line considered. The other symbols have their usual meaning. Lines that satisfy equation (2) are said to be on the linear part of their curve-of-growth. (For a derivation of this relation see, e.g., Spitzer 1978.) We will label an absorption line produced by an element Z in ionization stage i with rest transition wavelength λ and oscillator strength f as $Z^i_{\lambda,f}$.

For a metal absorption line of metallicity $[Z/H] \equiv \log{(n_Z/n_{\rm H})} - \log{(n_Z/n_{\rm H})_\odot}$ associated with a LYFA of hydrogen column density $N_{\rm HI}$ we now define the following quantity:

$$\mathrm{LOX}(Z^i_{\lambda,f}, [Z/H], N_{\rm HI}) \equiv -17.05 + \log N_{\rm HI} + \left[\frac{Z}{\rm H}\right] + \log{(f\,\lambda^2)} + \log\left(\frac{n_Z}{n_{\rm H}}\right)_\odot + \log\left(\frac{x^i_Z}{x^0_H}\right), \tag{3}$$

which we will call the *line observability index.* The inspiration for this definition comes from rewriting equation (2) with the column density of the absorbing metal ions expressed in terms of $N_{\rm HI}$, [Z/H], and the solar ratio of the number densities of metal and H atoms $(n_Z/n_{\rm H})_\odot$. The model-dependent ionization corrections are contained in the last term, which is a mean value of the ratio of the ionization fractions $x^i_Z = n^i_Z/n_Z$ of Z^i and H^0 in the region where the Lyα absorption arises. Equation (3) assumes units of cm^{-2} for $N_{\rm HI}$ and Å for λ; the choice of additive constant then implies LOX $= \log{(W_{r\lambda}/\,1\,m\text{Å})}$ for weak lines. The LOX can thus be used to rank metal lines in terms of strength, and it can be directly compared to the detection limit in spectra of a given quality. Computation of the LOX as a function of $[Z/H]$ and $N_{\rm HI}$ requires a model of the densities and temperatures within Lyα forest absorbers, which together with the ionizing background radiation field J_ν determine the ionization term x^i_Z/x^0_H as a function of $N_{\rm HI}$.

3. LOX for 2249 candidate metal lines

We have applied the LOX technique to two different cosmological simulations. One is the standard CDM simulation described in Davé et al. (1996). A box of length 22.222 comoving Mpc containing baryonic and dark matter is evolved from $z = 49$ to $z = 2$ using TreeSPH (Hernquist & Katz 1989), assuming a CDM spectrum of density fluctuations with the parameters $\sigma_{8h^{-1}} = 0.7$,

$\Omega = 1.0$, $h = 0.5$, $\Omega_b h^2 = 0.0125$, and $n = 1$, where $h \equiv \mathrm{H}_0/100$ km/s/Mpc and n is the slope of the initial perturbation spectrum. The other simulation, a flat, nonzero-Λ model, also assumes a CDM spectrum of density fluctuations, with $\sigma_{8h^{-1}} = 0.8$, $\Omega = 0.4$, $\Lambda = 0.6$, $h = 0.65$, $\Omega_b h^2 = 0.0125$, and $n = 0.93$. The standard model is inconsistent with the amplitude of CMB anisotropy measured by COBE (Smoot et al. 1992), but the normalization of the Λ model (computed using the CMBFAST program of Seljak & Zaldarriaga 1996) is matched to the 4-year COBE data. For further details regarding the simulation method, see Katz, Weinberg, & Hernquist (1996a).

The analysis of the two cosmological models yielded very similar results. The LOX is a local property, depending on the conditions within individual density peaks along the line of sight, which are insensitive to the underlying cosmology. Hence, in the following we will only describe the calculations for one of the models, the ΛCDM model, and we will focus on results at $z = 3$. A spatially uniform photoionizing background radiation field is imposed, with the shape computed by Haardt & Madau (1997, in preparation). They calculate the modification due to absorption and re-emission by the IGM of an input radiation field with $J_\nu \propto \nu^{-1.8}$ for $\lambda < 1050$Å, $J_\nu \propto \nu^{-0.9}$ for $1050\text{Å} \leq \lambda \leq 2200$Å, and $J_\nu \propto \nu^{-0.3}$ for $\lambda > 2200$Å. This radiation field, at $z = 3$, has a larger drop above the He^+ absorption edge at 4 Rd than the previously published Haardt & Madau spectrum (1996), by roughly a factor of three, and it is therefore in better agreement with the relatively large number of SiIV systems observed at that redshift (see the discussion in Hellsten et al. 1997).

To evaluate the ionization correction term in expression (3) we need to know the typical volume densities and temperatures in the absorbers for different values of N_{HI}. To find the relation between these quantities, we generated artificial Lyα absorption spectra along 480 lines of sight through the simulation box at $z = 3$, using the method described in Hellsten et al. (1997). The lines of sight were selected to include a relatively large number of the high-column density absorbers in order to get good statistics for these rather uncommon systems. We use artificial spectra along random lines of sight to fix the overall amplitude of the background radiation field, scaling J_ν by a constant factor so that the mean Lyα flux decrement in the simulated spectra matches the value $D_A = 0.36$ found by Press, Rybicki, & Schneider (1993; see further discussion by Rauch et al. 1997).

Figure 1 shows results from an analysis of 1456 HI absorption features detected in these artificial spectra. Lines are identified by a threshold criterion in the following way. First, we define the velocity interval from a position where the HI optical depth τ_α increases above a critical value $\tau_c = 1.2$ until it drops below that value again as belonging to an HI absorption feature. Next, we augment this interval on both sides until either $\tau_\alpha < 0.1$ or a local maximum in τ_α is encountered. This procedure separates weakly blended "W-shaped" absorption features, if $\tau_\alpha < \tau_c$ at the central local minimum.

The HI column density of the absorber is found by integration of τ_α over the velocity interval, i.e.

$$N_{\rm HI} \;=\; \frac{m_e c}{\pi e^2 f_\alpha \lambda_\alpha} \int_{\Delta v} \tau_\alpha(v)\, dv \;=\; 7.44 \times 10^{11}\,{\rm cm}^{-2} \int_{\Delta v} \tau_\alpha(v)\, dv, \qquad (4)$$

where v is measured in km/s in the rightmost expression. The crucial question for our purposes is the relation between $N_{\rm HI}$ and the typical volume density of gas in the absorbing region. Because of peculiar motions and Doppler broadening, the absorbing HI atoms in a given velocity bin originate at slightly different spatial locations. The code we developed to generate the artificial spectra also determines the *mean* total hydrogen volume density $n_{\rm H}(v)$ in the regions from which the HI atoms originate. In Figure 1 we plot $n_{\rm H}$ vs. $N_{\rm HI}$, where $n_{\rm H}$ is the maximum value of $n_{\rm H}(v)$ in the velocity interval Δv of that absorption feature. In the spectra, the location of this density peak is close to the location of the maximum of $\tau_\alpha(v)$, as one would expect.

As can be seen in Figure 1, there is a well-defined correlation between the HI column density of a LYFA and the typical total volume hydrogen density of the absorbing region. The thick solid line is the power-law fit

$$\log n_{\rm H} = -14.8 + \log \frac{\Omega_b h^2}{0.0125} + 0.7 \log N_{\rm HI}, \qquad (5)$$

which we will use to evaluate the LOX.

Relation (5) depends on the value of $\Omega_b h^2$, i.e., the total mean baryonic density. Increasing the value of $\Omega_b h^2$ will shift the curve upward if $N_{\rm HI}$ is held constant (to satisfy the mean flux decrement constraint) by adjusting the intensity of the UV radiation field. The indicated scaling with $\Omega_b h^2$ in (5) is only approximate, because it neglects effects of the temperature dependence on $\Omega_b h^2$ (Croft et. al. 1997). We will assume $\Omega_b h^2 = 0.0125$ throughout this paper, except for the discussion in Section 4. While a similar correlation between $n_{\rm H}$ and $N_{\rm HI}$ holds at other redshifts, the constant of proportionality is different because of the evolution in the radiation field and the IGM structure, in particular the dilution of the cosmic mean density by the expansion of the universe. The $n_{\rm H}$-$N_{\rm HI}$ correlation for the SCDM model is very similar, with a slope of about 0.73 instead of 0.7, and the resulting line observability indices are nearly identical for the two relations.

Also shown in Figure 1 is the mean total hydrogen density at $z = 3$ in this model. It is seen that the model predicts that LYFAs with $\log(N_{\rm HI}) \lesssim 14$ at $z = 3$ arise from underdense regions (similar to the result of Zhang et al. 1997).

The relation between density and temperature is slightly more complex. Figure 2 shows a plot of $n_{\rm H}$ versus mean temperature for the same density peaks as those shown in Figure 1. For low densities a large fraction of the peaks follow the relation $T \propto n_{\rm H}^{0.65}$. At densities $n_{\rm H} \lesssim 10^{-4}{\rm cm}^{-3}$, the density-temperature correlation arises mainly from the interplay between photoionization heating and adiabatic cooling due to the expansion of the universe. Low density regions have lower neutral fractions, hence lower photoionization heating rates, and they expand more rapidly, thus experiencing stronger adiabatic cooling. Some of the peaks lie above this temperature-density relation, at $T \sim 10^{4.5-5}$K, because of moderate shock heating. Peaks with $\log n_{\rm H} \gtrsim -3.6$ have large enough densities for radiative cooling to become significant, and the temperature is roughly determined by the equilibrium between radiative cooling and photoionization heating. (For a more detailed discussion of the density-temperature relation in cosmological simulations, see, e.g., Croft et al. 1997; Hui & Gnedin 1997; Zhang et al. 1997). For our LOX calculations we will adopt the relation defined by the solid line in Figure 2. This relation is again very similar to that in the SCDM model, although the latter shows a slightly larger scatter at lower densities. Because photoionization is the main source of ionization at such low densities, the LOX is insensitive to the exact value of the temperature.

For an arbitrary metal line $Z^{i}_{\lambda,f}$ associated with a LYFA with neutral column density $N_{\rm HI}$ and metallicity [Z/H], we can now evaluate the ionization correction term in (3) using the photoionization code CLOUDY 90 (Ferland 1996). The inputs to CLOUDY are the hydrogen volume density and the temperatures from the relations discussed above, as well as the UV radiation field. For systems with $\log N_{\rm HI} \gtrsim 16$, continuum HeII absorption affects the radiation field in the central regions of the absorbers. We include this effect in an approximate way, by solving self-consistently for the radiative transfer through a plane parallel slab with HI column density $2 \times N_{\rm HI}$, illuminated from both sides. We then use the volume averaged values of the ionization fractions, which should roughly be equal to those in the central region of an absorber with HI column density $N_{\rm HI}$. Including this HeII-shielding effect only changes the predicted LOX values slightly.

The results in Table 1 are produced by evaluating the LOX for the 2249 transitions in the compilation by Verner, Barthel, and Tytler (1994) and then sorting the lines according to the observability index. The strongest lines are shown for five different values of the HI column density, $\log N_{\rm HI} = 13$, 14, 15, 16, and 17. We show, for $\log N_{\rm HI} > 14$, only the ten strongest lines with $\lambda_r < 912$Å. These extreme ultraviolet lines are numerous, but in spectra of the faint QSOs at $z \sim 3$ they are extremely difficult to detect, even with state of the art instruments such as the Space Telecope Imaging Spectrograph, installed on the Hubble Space Telescope (HST) in February 1997 (e.g. Danks et al. 1996). At somewhat lower redshifts, the prospects should be better for observing these lines in STIS spectra of a few very bright QSOs, such as HE 2347+4342 (z=2.88, Reimers et al. 1997), but the observations have yet to be made. With the Cosmic Origins Spectrograph (COS), scheduled to be installed on the HST in 2002 (Green et al. 1997), detection of these important lines may finally become possible for a larger number of QSOs at high redshift.

A metallicity of $[{\rm O/H}] = -2.5$ has been assumed in Table 1, and we use the solar metallicity values from Grevesse & Anders (1989). We evaluate the LOX for solar *relative* abundances, i.e. [Z/O]=0. It can then be scaled to any other relative abundance pattern a posteriori. For example, if [O/C]=0.5, as observed in some low metallicity systems (e.g. Wheeler et al. 1989), we have to add 0.5 to the LOX values for O lines, (i.e. use [O/H]=-2) in order to compare them to the C lines for [C/H]=-2.5.

Before discussing the results in Table 1, let us estimate detection limits in present day, high signal-to-noise ratio (S/N) HIRES spectra. For a line with rest frame wavelength λ_r, the rest equivalent width threshold for an N_σ-sigma detection is

$$\mathrm{W}_r(N_\sigma) \;=\; \frac{N_\sigma \lambda_r \sqrt{N_{\rm pix}}}{\mathrm{S/N}}(\Delta v_{\rm pix}/c) \;=\; \frac{N_\sigma \sqrt{N_{\rm pix}}\,\Delta\lambda_{\rm pix}}{\mathrm{S/N}\,(1+z_{\rm abs})}, \qquad (6)$$

where $N_{\rm pix} = 7$ is the number of pixels used for the equivalent width detection limit and $\Delta v_{\rm pix}$ ($\Delta\lambda_{\rm pix}$) is the velocity (wavelength) spread per pixel (Churchill 1997). For the spectrum of Q1422+231 obtained by SC, $\Delta\lambda = 0.06$Å and $z_{\rm abs} \approx 3$. Hence lines with LOX $\gtrsim (2.3 - \log \mathrm{S/N})$ should be detectable at the 5-sigma level in that spectrum. (Recall from §2 that $W_r = 1\text{mÅ} \times 10^{\rm LOX}$ for weak lines.) The S/N per pixel is roughly 110 outside the Lyα forest and 45 within the forest, which translates into a minimum detectable LOX of approximately 0.26 outside the forest and 0.65 within the forest. The integration time for this spectrum was 8.2 hrs. If the QSO is observed for 3-4 nights the S/N ratio could be roughly doubled, so a practical absolute lower limit for observable lines would be LOX $\gtrsim 0$.

Looking at Table 1, the OVI(1032,1038) doublet is predicted to be a dominant metal line feature associated with LYFAs with $\log N_{\rm HI} = 13$, 14, and 15. For [O/H]=-2, OVI(1032) becomes observable for $\log N_{\rm HI} \gtrsim 13$ and tops the list for more than two orders of magnitude in $N_{\rm HI}$. Because this OVI doublet has rest wavelengths less than 1216 Å, the absorption features will always be located in the Lyα forest where they are subject to heavy blending and blanketing by HI lines, making them difficult to identify, especially in high redshift spectra.

A family of strong absorption lines from lower ionization states of oxygen is seen to be present for the higher column density LYFAs. These lines all have $\lambda_r \leq 833$Å, and cannot (for $z \lesssim 4-5$) be observed in the optical. They present a challenge for the next generation of ultraviolet spectrographs.

For lines with $\lambda_r > 1216$Å, the CIV(1548,1551) doublet is seen to be dominant over the entire range of HI column densities, a remarkable result, given that this range in $N_{\rm HI}$ spans three orders of magnitude in volume density and hence photoionization parameter. Only for HI column densities close to that of Lyman limit systems ($\log N_{\rm HI} \gtrsim 17.2$) do other metal lines, such as the SiIV(1394,1403) doublet, attain strengths comparable to that of CIV. This prediction is consistent with the fact that the first metal lines found to be associated with LYFAs were CIV lines, and that CIV systems are the best studied and most numerously observed metal line systems to date.

The lines with $\lambda_r > 912$Å reaching the largest LOX values are CIII(977) and SiIII(1206). In the high column density LYFAs these lines are predicted to be so strong that the prospects of detecting them in the Lyα forest should be reasonable, and they have indeed been observed in a few LYFAs in the Q1422 spectrum (SC 96). These lines deserve a more thorough investigation with artificial absorption spectra. A good way of testing simulation predictions for high column density LYFAs would be to compare CIII absorption in real spectra to the CIII features in a model with [C/H] determined observationally from the corresponding CIV features.

Figures 3 and 4 show graphical representations of the $N_{\rm HI}$-LOX relations for 12 lines selected from Table 1. In low density regions, the LOX is insensitive to the scatter in gas temperature, because photoionization is much more important than collisional ionization and because the recombination coefficients are not very temperature sensitive. A more complicated issue is what would happen if the *mean* temperature of the low density gas were different in the model, for example because of a different assumption about the heat input during the reionization period (Hui & Gnedin 1997; Rauch et al. 1997). The effect on the LOX is small in this case also, as we will argue in detail in Section 4.

Figure 3 contains lines from three different ionization states of carbon and silicon. The CIV(1548), CIII(997), and CII(1335) lines are expected to be observable in absorbers with $\log N_{\rm HI} \gtrsim 14$, 14.9, and 15.8, respectively. These values are obtained assuming a resolution and S/N similar to that of SC's spectrum of Q1422+231, and a metallicity of [O/H]=-2.5. It is straightforward to predict these values for spectra of other resolutions and signal-to-noise ratios by means of equation (6), and for other metallicities by shifting the LOX-curves upwards by an amount Δ(LOX) = [O/H]+2.5 (or alternatively sliding the horizontal detection limit lines downwards by the same amount). For example, for CIV to be detectable in a LYFA with $N_{\rm HI} = 10^{13}\,{\rm cm}^{-2}$ in the SC spectrum, one can estimate from Figure 3 that [O/H] would have to be $\gtrsim -0.8$.

The diagonal arrows on Figure 3 indicate how the curves will shift if J_ν is multiplied by a factor of 2 (solid arrow) or if $\Omega_b h^2$ is changed from 0.0125 to 0.02 and J_ν is adjusted to maintain the observed D_A (dashed arrow). The direction and magnitude of these arrows can be derived from approximate scaling laws, as will be discussed in Section 4.

The modeling of the ionization correction term in the LOX is based on a single-density model, assuming that most of the absorption takes place at or near the maximum of the local density peak associated with a LYFA. This is certainly true for HI. As long as the volume density of a species Z^i increases with total density (i.e. the LOX increases with $N_{\rm HI}$) this assumption holds. In situations where Z^i decreases with total density this approximation becomes worse. For example, in our artificial spectra we sometimes see that the CII(1335) feature associated with a high column density absorber ($\log N_{\rm HI} \sim 16.5$) is centered on the same velocity as HI, whereas the corresponding CIV (or OVI) absorption is seen as shoulders that are offset relative to the HI feature. This occurs because the CIV density profile does not follow that of the total density. Therefore, our maximum density assumption causes us to underestimate the LOX values on the decreasing parts of the curves in Figures 3-4. They are lower limits to the true LOX values, and it is necessary to do a full generation and analysis of artificial spectra if one wants to use, say, observed CII/CIV ratios to infer ionization properties of the IGM. Direct comparison to the LOX values in Figure 3 would overestimate the photoionization parameter in the central region of the LYFA.

Figure 3 also shows the silicon lines SiIV(1394), SiIII(1206), and SiII(1260). Here, the SiIV and SiIII features are observable only for $\log N_{\rm HI} \gtrsim 15.8$, and the SiII feature for $\log N_{\rm HI} \gtrsim 16.3$. In addition, the SiII line falls redward of the Lyα forest only for LYFAs close to the Lyα emission peak. Clearly, for most LYFAs these silicon lines are not as promising for probing ionization conditions as the carbon lines discussed above.

Lines from the family of very strong O transitions OIII(833), OIV(788), OV(630), and OVI(1032), as well as NV(1239) and SVI(1063), are displayed in Figure 4. OVI is by far the strongest 'high ionization' line with $\lambda_r > 912$Å, and it is observable in the entire interval $13.6 \lesssim \log N_{\rm HI} \lesssim 15.8$. For systems with $\log N_{\rm HI} \approx 14.5$, OVI should be detectable in the SC spectrum, provided $[{\rm O/H}] \gtrsim -3$. In our model, the OVI is produced mainly from photoionization, and the LOX is not very sensitive to the assumed temperature. With present day spectra, OVI is the best and only candidate for probing the metallicity of the IGM in regions close to the mean density. As we already mentioned, observations of the OVI lines are hampered by the high line density within the Lyα forest. Low column density lines in cosmological simulations are usually broadened by Hubble flow and peculiar velocities rather than thermal motions, so the OVI lines may not necessarily be distinguishable by low b-parameters. In individual cases, however, it should at least be possible to place upper limits to the metallicity of the systems that happen not to have strong HI contamination at the expected positions of the OVI features.

The NV(1239,1243) is predicted to be weaker than the OVI doublet and probe a somewhat denser part of the IGM. If [N/C] is as low as -0.7 as suggested by Pettini et al. (1995) the NV doublet will be observable only in LYFAs with relatively high metallicity, roughly $[{\rm O/H}] \gtrsim -1.8$. This seems consistent with the fact that SC observed NV in only one out of six candidate absorbers in their Lyβ selected sample.

Towards lower redshifts, where the Lyα forest begins to thin out, it should become increasingly easy to identify OVI absorption lines by their coincidence with corresponding Lyα and Lyβ absorption, at least in a statistical way. Though somewhat arduous, this type of investigation with OVI is probably the most promising route to testing the trend between metallicity and HI column density predicted by some models of early IGM enrichment (e.g., Gnedin & Ostriker 1997).

4. LOX dependence on model parameters

Figures 3 and 4 present LOX results for a single redshift and a single set of model parameters: ΛCDM at $z = 3$, with $\Omega_b h^2 = 0.0125$ and the Haardt-Madau (1997) UV background spectrum scaled in intensity to give an HI photoionization rate $\Gamma_{\rm HI}$ such that $D_A = 0.36$ in the simulated spectra. However, we can estimate the effects of changing some of these parameters by simple scaling arguments because the dynamics of the gas in the density regime relevant to LYFAs is driven by the gravity of the dark matter, making the spatial distribution of the gas insensitive to changes in Ω_b, J_ν, or the IGM temperature. We can therefore compute the effects of such changes on the $N_{\rm HI}$ vs. $n_{\rm H}$ correlation (Figure 1), and we can compute the effect on LOX values through equation (3) if we make the approximation that the ionization fractions x_Z^i depend only on the ionization parameter $\Gamma/n_{\rm H}$. Because recombination rates vary only slowly with temperature and the range of temperatures in LYFAs is much smaller than the range of densities, this is a good, but not a perfect, approximation.

Consider first the effect of changing J_ν by a constant factor q. This change in isolation would alter the mean flux decrement D_A, which we have thus far adopted as an observational constraint on the model, but current observational uncertainties in D_A allow some range in J_ν (compare, e.g., Zuo & Lu 1993 to Press et al. 1993 and Rauch et al. 1997), and comparison of simulated and observed HI column density distributions favors a somewhat higher value of J_ν than we have adopted here (Davé et al. 1997; Gnedin 1997a). We assume that the shape of J_ν does not change, so that the photoionization rates Γ for all species change by the same factor. An absorber that previously had column density $N'_{\rm HI}$ now has a column density $N_{\rm HI} = q^{-1}N'_{\rm HI}$ — raising J_ν lowers the hydrogen neutral fraction and therefore lowers $N_{\rm HI}$. The density $n_{\rm H}$ in this absorber is the same as before, so the ionization parameters $\Gamma/n_{\rm H}$ are the same as those in an absorber that previously had column density $N''_{\rm HI} = q^{-1.43}N'_{\rm HI} = q^{-0.43}N_{\rm HI}$. We have used the correlation $n_{\rm H} \propto {N_{\rm HI}}^{0.7}$ from Figure 1 to convert a factor q^{-1} change in $n_{\rm H}$ to a factor $q^{-1.43}$ change in $N_{\rm HI}$. Assuming that $\log(x_Z^i/x_H^0)$ depends only on $\Gamma/n_{\rm H}$, we see from equation (3) that

$$\mathrm{LOX}(qJ_\nu, \log N_{\rm HI}) = \mathrm{LOX}(J_\nu, \log N_{\rm HI} - 0.43\log q) + 0.43\log q, \qquad (7)$$

where the second term accounts for the difference $\log N_{\rm HI} - \log N''_{\rm HI}$. For example, the effect of doubling J_ν while keeping other parameters fixed is to shift the LOX($\log N_{\rm HI}$) curves diagonally by the vector (0.13,0.13), indicated by the solid arrow in Figure 3. The magnitude of this shift is small, and the direction is nearly parallel to the LOX curve itself. The same shift would apply to Figure 4.

If we keep J_ν fixed but change Ω_b by a factor q, then absorber densities $n_{\rm H}$ change by q and column densities by q^2 (because the hydrogen neutral fraction is itself proportional to $n_{\rm H}$). An absorber that previously had column density $N'_{\rm HI}$ now has $N_{\rm HI} = q^2 N'_{\rm HI}$. The ionization parameters are the same as those in an absorber that previously had column density $N''_{\rm HI} = q^{1.43}N'_{\rm HI} = q^{-0.57}N_{\rm HI}$. With the same reasoning as before, we find

$$\mathrm{LOX}(q\Omega_b, \log N_{\rm HI}) = \mathrm{LOX}(\Omega_b, \log N_{\rm HI} + 0.57\log q) - 0.57\log q, \qquad \text{fixed } J_\nu. \qquad (8)$$

Since the observational constraints on D_A are better than those on the ionizing background intensity, a factor q change in Ω_b should really be accompanied by a factor q^2 change in J_ν, so that D_A and the HI column densities of absorbers remain the same. The net change is to increase $\Gamma/n_{\rm H}$ by a factor of q at fixed $N_{\rm HI}$. An absorber with column density $N_{\rm HI}$ has the same ionization parameters as an absorber that previously had column density $N''_{\rm HI} = q^{-1.43}N_{\rm HI}$. Thus,

$$\mathrm{LOX}(q\Omega_b, q^2 J_\nu, \log N_{\rm HI}) = \mathrm{LOX}(\Omega_b, J_\nu, \log N_{\rm HI} - 1.43\log q) + 1.43\log q, \qquad \text{fixed } D_A. \qquad (9)$$

For example, the dashed arrow in Figure 3 shows the effect of increasing Ω_b from the value $\Omega_b = 0.03$ used in our simulation to the value $\Omega_b = 0.047$ favored (for $h = 0.65$) by the low [D/H] value of Tytler et al. (1996).

Plausible variations in the assumed gas reionization history can alter the temperature of the low density IGM by factors $\sim 2 - 3$ (Miralda-Escudé & Rees 1994; Hui & Gnedin 1997). Because the HI recombination coefficients are $\propto T^{-0.7}$ for $T \sim 10^4$ K, a factor q change in gas temperatures requires a factor $q^{-0.7}$ change in J_ν to keep D_A fixed. From the scaling relation (7), we see that the impact of such a temperature change would be small.

To estimate the evolution of the LOX with redshift, we can appeal to the argument of Hernquist et al. (1996) and Miralda-Escudé et al. (1996) that the primary driver of evolution in the Lyα forest at high redshift is the expansion of the universe, which changes the cosmic mean density in proportion to $(1+z)^3$. Non-linear gravitational evolution changes the overdensity field $\rho/\overline{\rho}$, but this evolution has a smaller impact on the forest than the overall expansion, at least for low column density absorbers. Matching the observed evolution of D_A requires an HI photoionization rate $\Gamma_{\rm HI}$ that is roughly constant between $z = 4$ and $z = 2$ (Hernquist et al. 1996; Miralda-Escudé et al. 1996; Rauch et al. 1997), so if we ignore changes to the shape of the spectrum we can take J_ν to be constant over this interval. A factor of two *decrease* in $(1+z)^3$ — roughly the change between $z = 4$ and $z = 3$ or between $z = 3$ and $z = 2$ — has the same effect as a factor of two *increase* in J_ν at a given redshift, illustrated by the solid arrow in Figure 3. While this argument is only approximate, it is enough to show that the LOX should not vary strongly with redshift over the range $z = 2 - 4$, except in the case of ionic species that are affected by the change in the spectral shape of J_ν.

Structure formation models that have a power spectrum amplitude similar to that of ΛCDM on Mpc scales at $z = 3$ will predict similar spatial and density structure in the diffuse IGM. (Models with very different power spectra will of course predict different structure, but such models may soon be ruled out by the Lyα forest data themselves [see, e.g., discussions by Rauch et al. 1997; Gnedin 1997b; Croft et al. 1998].) If the baryon density $\Omega_b h^2$ is held fixed, then the most important effect of changing the cosmological model is to alter the expansion rate $H(z)$. Matching D_A requires $\Gamma_{\rm HI} \propto H^{-1}(z)$ (see, e.g., equation [2] of Rauch et al. 1997), so halving $H(z)$ has the same impact as doubling J_ν. In practice the difference between $H(z)$ values in currently popular models at $z \sim 3$ is less than a factor of two, so the expected impact is small.

We conclude that our quantitative predictions for the LOX are likely to hold rather generally in the cosmological picture of LYFAs, at least for column densities $N_{\rm HI} \lesssim 10^{15}$ cm^{-2}, where the scaling arguments used in this Section are most secure. Our comparison of two numerical simulation models, a standard CDM model and a ΛCDM model, supports this claim, and it does not show any major changes to the LOX predictions even for higher column densities. Of course, the LOX is always directly affected by the metallicity of the absorbing gas (equation [3]), and the insensitivity to cosmology implies that absorption observations can therefore yield robust estimates of the metallicity in different regions of the IGM. Ionization corrections are essential in the interpretation of such measurements, but the corrections are not strongly dependent on the assumed cosmological model.

5. Discussion

In this paper we have introduced the LOX, a measure that allows a comprehensive selection of the metal lines that are useful for testing the detailed predictions of models for LYFAs. We have applied this method to a particular model, a cosmological ΛCDM simulation, and we have quantitatively discussed the dependence of the results on the model parameters J_ν, Ω_b, and z. We have also performed this analysis for a different cosmological simulation, a standard CDM model, but the results differ negligibly from those of the ΛCDM model.

We find that very few detectable metal lines are associated with the low to moderate density regions of the IGM that give rise to absorbers with $\log N_{\rm HI} \lesssim 15$. Most of the baryons in the Universe at $z = 3$ are believed to reside in this part of the IGM (e.g., Zhang et al. 1997), and the OVI(1032,1038) doublet is found to be the best probe of the metallicity in these regions. Other strong O lines, such as OV(630), OIV(788), and OIII(833) are technically difficult to observe, and have yet to be detected. The CIII(977) and SiIII(1206) lines are the strongest metal lines in high column density LYFAs. The CIV(1548) line is the strongest metal line with $\lambda_r > 1216$Å for all LYFAs with $\log N_{\rm HI} \lesssim 17$. While the specific values of the LOX as a function of column density will depend on redshift and on the adopted cosmological model and radiation field, we have argued that the qualitative conclusions presented above are insensitive to the choice of cosmological model of high redshift LYFAs, and they should hold generally within this scenario.

The relatively uncommon absorbers with $\log N_{\rm HI} \gtrsim 16$ should offer the strongest test of cosmological simulations. These systems should have more than a dozen observable metal lines associated with them (for [O/H] ~ -2.5). The relative strengths of these lines will depend on the assumed radiation field and abundance pattern, so a first check would be whether it is possible to make the line strengths in the model spectra match those of lines associated with high column density LYFAs for reasonable values of model parameters. Then one should make a detailed examination of the relative locations in velocity space between absorption components of individual species. A detailed comparison to observations will ultimately determine if the resolution of the simulations is adequate in these high-density regions, and to what extent local dynamical effects associated with the production of metals can be neglected. There are some hints of discrepancies between models and observations for these high column density systems. For example, the models in some cases predict the velocity components of CIV and CII absorption lines to differ, whereas there seems to be some new observational evidence that CII and CIV components are found at the same positions (A. Boksenberg, private communication).

Cosmological simulations depict the typical low column density LYFAs as simple structures:

low density, smooth, and governed by the straightforward physics of gravity, cosmic expansion, and photoionization. Studies of absorption along parallel lines of sight provide direct observational support for this point of view, especially recent HIRES observations of gravitationally lensed QSOs that set stringent lower limits to the scale of any substructure within low column density absorbers (Rauch 1997; see also Smette et al. 1992, 1995). The simulations do not predict a sudden change in LYFA properties at any particular column density, but they do predict a steady increase of gas density with $N_{\rm HI}$ (Fig. 1). For $\log N_{\rm HI} \gtrsim 16$, the typical absorbers are partially collapsed structures, and gas within them has begun to experience radiative cooling. In this regime, the finite mass and spatial resolution of the simulations may limit the accuracy of the results, and local astrophysical processes such as star formation and supernova explosions might influence the structure of these systems. The standard CDM model studied here produces only about 1/3 of the observed number of Lyman limit systems ($\log N_{\rm HI} \geq 17.2$), even though it matches the abundance of much stronger, damped Lyα absorbers quite well (Katz et al. 1996b; Gardner et al. 1997). While further work is needed to assess the sensitivity of this result to cosmological parameters — especially the baryon density parameter Ω_b — the discrepancy of numbers suggests that a population of absorbers unresolved by the simulations may become important at column densities $\log N_{\rm HI} \sim 17$.

The high column density LYFAs in the cosmological simulations represent the transition between the weak IGM fluctuations traced by low column density lines and the cold gas concentrations in virialized dark halos traced by damped Lyα absorption. The high-LOX lines listed in Table 1 can reveal many details of the structure and physical conditions in these absorbers, testing the accuracy of the simulations in this regime, providing clues to the nature of any additional absorber populations, and capturing snapshots of gas as it makes its way from the IGM into high redshift galaxies.

Acknowledgements

We thank the referee for drawing our attention to the importance of the absorption lines in the extreme UV. UH acknowledges support by a postdoctoral research grant from the Danish Natural Science Research Council. This work was supported by the NSF under grant ASC93-18185 and the Presidential Faculty Fellows Program and by NASA under grants NAG5-3111, NAG5-3525, and NAG5-3922. Computing support was provided by the San Diego Supercomputer Center.

REFERENCES

Bi, H.G., & Davidsen, A. 1997, ApJ, 479, 523

Cen, R., Miralda-Escudé, J., Ostriker, J.P., & Rauch M. 1994, ApJ, 437, L9

Churchill, C. 1997, Ph.D. Thesis, Univ. of California, Santa Cruz.

Cowie, L.L., Songaila, A., Kim, T.-S., & Hu, E.M. 1995, AJ., 109, 1522

Croft, R.A.C., Weinberg, D.H., Katz, N., & Hernquist, L. 1997, ApJ, in press

Croft, R.A.C., Weinberg, D.H., Katz, N., & Hernquist, L. 1998, ApJ, submitted

Danks, A., Woodgate, B., Kimble, R., Bowers, C., Grady, J., Kraemer, S., Kaiser, M.E., Meyer, W., Hood, D. & van Houten, C. 1996, in Science with the HST-II, Space Telescope Science Institute, eds. Benvenuti, Macchetto & Schreier.

Davé, R., Hernquist, L., Weinberg, D.H., & Katz, N. 1997, ApJ, 477, 21

Ferland, G.J., 1996, University of Kentucky, Department of Astronomy, Internal report

Gardner, J.P., Katz, N., Hernquist, L., & Weinberg, D.H. 1997, ApJ, in press (astro-ph/9609072)

Gnedin, N. Y. 1997a, MNRAS, submitted (astro-ph/9707257)

Gnedin, N. Y. 1997b, MNRAS, submitted (astro-ph/9706286)

Gnedin, N. Y. & Ostriker, J. P., ApJ, submitted, astro-ph/9612127

Green, J., Shull, J.M., Morse, J. et al. 1997, proposal for "Cosmic Origins Spectrograph", selected by NASA for Hubble Space Telescope 2002 Refurbishment Mission.

Grevesse, N. & Anders, E. 1989, Cosmic Abundances of Matter, AIP Conf. Proceedings 183,1.

Gunn, J.E. & Peterson, B. A. 1965, ApJ, 142, 1633

Haardt, F. & Madau, P. 1996, ApJ, 461, 20

Haardt, F. & Madau, P. 1997, in prep.

Haehnelt, M.G., Steinmetz, M., & Rauch, M. 1996, ApJ, 465, L65

Hernquist, L. & Katz, N. 1989, ApJS, 70, 419

Hellsten, U., Davé, R., Hernquist, L., Weinberg, D. & Katz, N. 1997, ApJ, vol. 487

Hernquist, L., Katz, N., Weinberg, D.H., & Miralda-Escudé, J. 1996, ApJ, 457, L51

Hui, L., Gnedin, N., 1997, MNRAS, submitted, astro-ph/9612232

Katz, N., Weinberg, D.H., & Hernquist, L. 1996a, ApJS, 105, 19

Katz, N., Weinberg D.H., Hernquist, L., & Miralda-Escudé, J. 1996b, ApJ, 457, L57

Lu, L. 1991, ApJ, 379, 99

Meyer, D.M. & York, D.G. 1987, ApJ, 315, L5

Miralda-Escudé, J., Cen, R., Ostriker, J.P. & Rauch, M. 1996, ApJ, 471, 582

Miralda-Escudé J., & Rees, M. J. 1994, MNRAS, 266, 343

Petitjean, P., Mücket, J.P. & Kates, R.E. 1995, A&A, 295, L9

Pettini, M., Lipman, K., & Hunstead, R.W. 1995, ApJ, 451, 100

Press, W.H., Rybicki, G.B., & Schneider, D.P. 1993, ApJ, 414, 64

Rauch, M. 1997, in Proc. of the 13th IAP Colloquium, Structure and Evolution of the IGM from QSO Absorption Line Systems, eds. P. Petitjean & S. Charlot, (Paris: Nouvelles Frontières), astro-ph/9709129

Rauch, M., Haehnelt, M.G., & Steinmetz, M. 1996, ApJ, 481, 601.

Rauch, M., Miralda-Escudé, J., Sargent, W.L.W., Barlow, T.A., Weinberg, D.H., Hernquist, L., Katz, N.S. & Ostriker, J.P. 1997, ApJ, in press, astro-ph/9612245.

Reimers, D., Köhler, S., Wisotzki, L., Groote, D., Rodriguez-Pascual, P., & Wamsteker, W. 1997, A & A, 327, 890.

Seljak, U. & Zaldarriaga, M., 1996, ApJ, 469, 437

Smette, A., Surdej, J., Shaver, P. A., Foltz, C. B., Chaffee, F. H., Weymann, R. J., Williams, R. E., Magain, P. 1992, ApJ, 389, 39

Smette, A., Robertson, J. G., Shaver, P A., Reimers, D., Wisotzki, L., Koehler, T. 1995, A&AS, 113, 199

Smoot, G. F., et al. 1992, ApJ, 396, L1

Songaila, A. & Cowie, L. L. 1996, AJ, 112, 335 [SC]

Spitzer, L. Jr., 1978, Physical Processes in the Interstellar Medium, Wiley-Interscience.

Tytler, D., Fan, X.-M., and Burles, S. 1996, Nature, 381, 207

Verner, D.A., Barthel, P.D., & Tytler, D. 1994, A&AS, 108, 287

Wheeler, J.C., Sneden, C., & Truran, J.W. 1989, ARA & A, 27, 279

Womble, D.S., Sargent, W.L.W., & Lyons, R.S. 1995, in Cold Gas at High Redshift, eds. M. Bremer et al., Kluwer 1996, (astro-ph/9511035).

Zhang, Y., Anninos, P., & Norman, M.L. 1995, ApJ, 453, L57

Zhang, Y., Meiksin, A., Anninos, P., Norman, M.L., 1997, ApJ, in press (astro-ph 9706087).

Zuo, L., & Lu, L. 1993, ApJ, 418, 601

This preprint was prepared with the AAS LaTeX macros v4.0.

Fig. 1.— Maximum total hydrogen number density in units of $\log(\mathrm{cm}^{-3})$ versus the HI column density in units of $\log(\mathrm{cm}^{-2})$ for 1456 HI absorption features along 480 lines of sight at $z = 3$ in our cosmological model. The solid line shows the fit $\log n_{\mathrm{H}} = -14.8 + 0.7 \log N_{\mathrm{HI}}$. Also shown is the mean hydrogen density at $z = 3$ (dashed line).

Fig. 2.— Temperature vs. hydrogen number density for the same density peaks as plotted in figure 1. The shown fit is described by $T = 7.17 + 0.65 \log n_{\mathrm{H}}$ for $\log T < -3.8$ and $T = 3.18 - 0.4 \log n_{\mathrm{H}}$ for $\log T > -3.8$.

Fig. 3.— LOX(N_{HI}) for CIV(1548), CIII(977), and CII(1335) (solid curves) and SiIV(1394), SiIII(1207), and SiII(1260) (dashed curves) at $z = 3$, assuming [O/H] $= -2.5$. The horizontal lines are approximate detection limits within the Lyα forest (dashed line) and redwards of the forest (solid line) in Songaila and Cowie's spectrum of Q1422+231 (equation (6)). Arrows indicate the effects of doubling the radiation intensity (solid arrow) and of changing $\Omega_b h^2$ from 0.0125 to 0.02, as discussed in Section 4.

Fig. 4.— LOX(N_{HI})for OVI(1032), OV(630), OIV(788), and OIII(833) (solid curves), and NV(1243), and SVI(933) (dashed curves).

Table 1: LOX sorted lines for five different values of $\log N_{\rm HI}$

$\log N_{\rm HI}$ = **13**		**16**		**17**	
Line	LOX	Line	LOX	Line	LOX
OVI(1032)	0.21	CIII(977)	2.52	CIII(977)	2.98
OVI(1038)	-0.08	CIV(1548)	2.32	OIII(833)	2.43
OV(630)	-0.55	OIV(788)	2.07	OIII(702)	2.39
NV(1238)	-0.90	OIV(554)	2.07	SiIII(1207)	2.35
CIV(1548)	-0.94	CIV(1551)	2.02	OIII(507)	2.24
14		OIII(833)	1.95	OIII(306)	2.21
OVI(1032)	1.03	NIV(765)	1.92	CIV(1548)	2.16
OV(630)	0.74	OIII(702)	1.91	CIV(1551)	1.86
OVI(1038)	0.74	OV(630)	1.82	OIII(303)	1.74
CIV(1548)	0.33	OIV(553)	1.77	NIV(765)	1.69
NV(1239)	0.13	OIII(507)	1.76	NIII(686)	1.68
CIV(1551)	0.03	OIII(306)	1.73	NIII(990)	1.66
NV(1243)	-0.17	OIV(238)	1.69	CIII(386)	1.66
OIV(788)	-0.29	NIII(990)	1.29	OIII(374)	1.62
15		NV(1239)	0.81	SiIV(1394)	1.54
OV(630)	1.81	SiIII(1207)	0.80	SIII(678)	1.52
CIV(1548)	1.42	NV(1243)	0.52	OIII(267)	1.49
OVI(1032)	1.39	OVI(1032)	0.49	SiIV(1403)	1.25
OIV(788)	1.26	CII(1335)	0.47	MgII(2796)	1.16
OIV(554)	1.26	SiIV(1394)	0.40	AlII(1671)	1.10
CIV(1551)	1.12	SIV(1063)	0.30	CII(1335)	1.08
NIV(765)	1.11	CII(1036)	0.23	SiII(1260)	1.03
OVI(1038)	1.09	OVI(1038)	0.19	MgII(2804)	0.85
OIV(553)	0.96	SiIV(1403)	0.10	CII(1036)	0.84
NV(1239)	0.90	SIII(1013)	0.01	SiII(1193)	0.68
OIV(238)	0.88			SiII(1190)	0.38
OIV(608)	0.82			AlIII(1855)	0.35
CIII(977)	0.77			SIV(1063)	0.32
NV(1243)	0.60			SIII(1013)	0.27
NeV(568)	0.27			SiII(1527)	0.25
OIII(833)	0.26			SIII(1190)	0.19
OIII(702)	0.22			AlIII(1863)	0.05

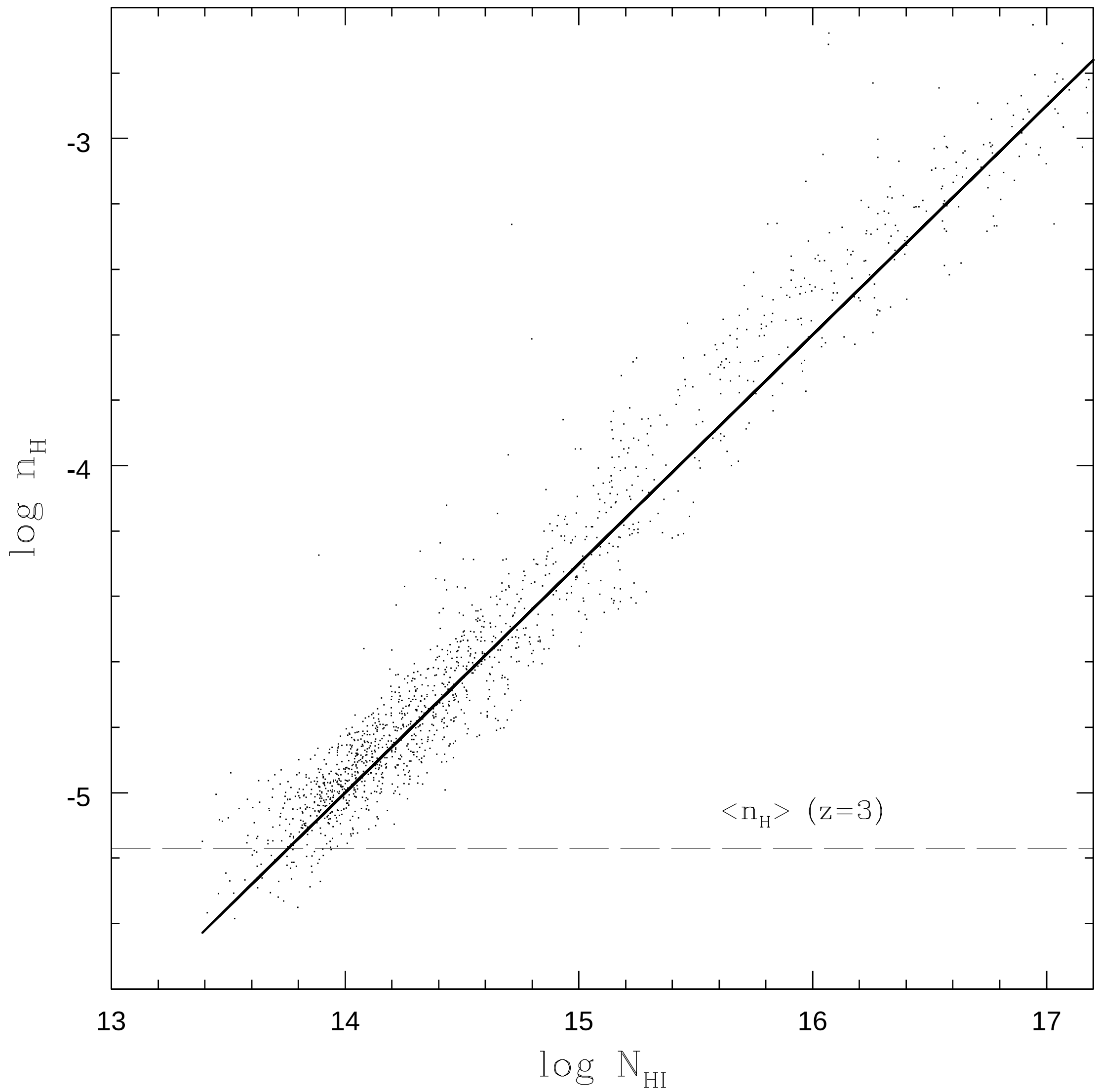

-3
-4
-5
log n_H
<n_H> (z=3)
13
14
15
16
17
log N_{HI}

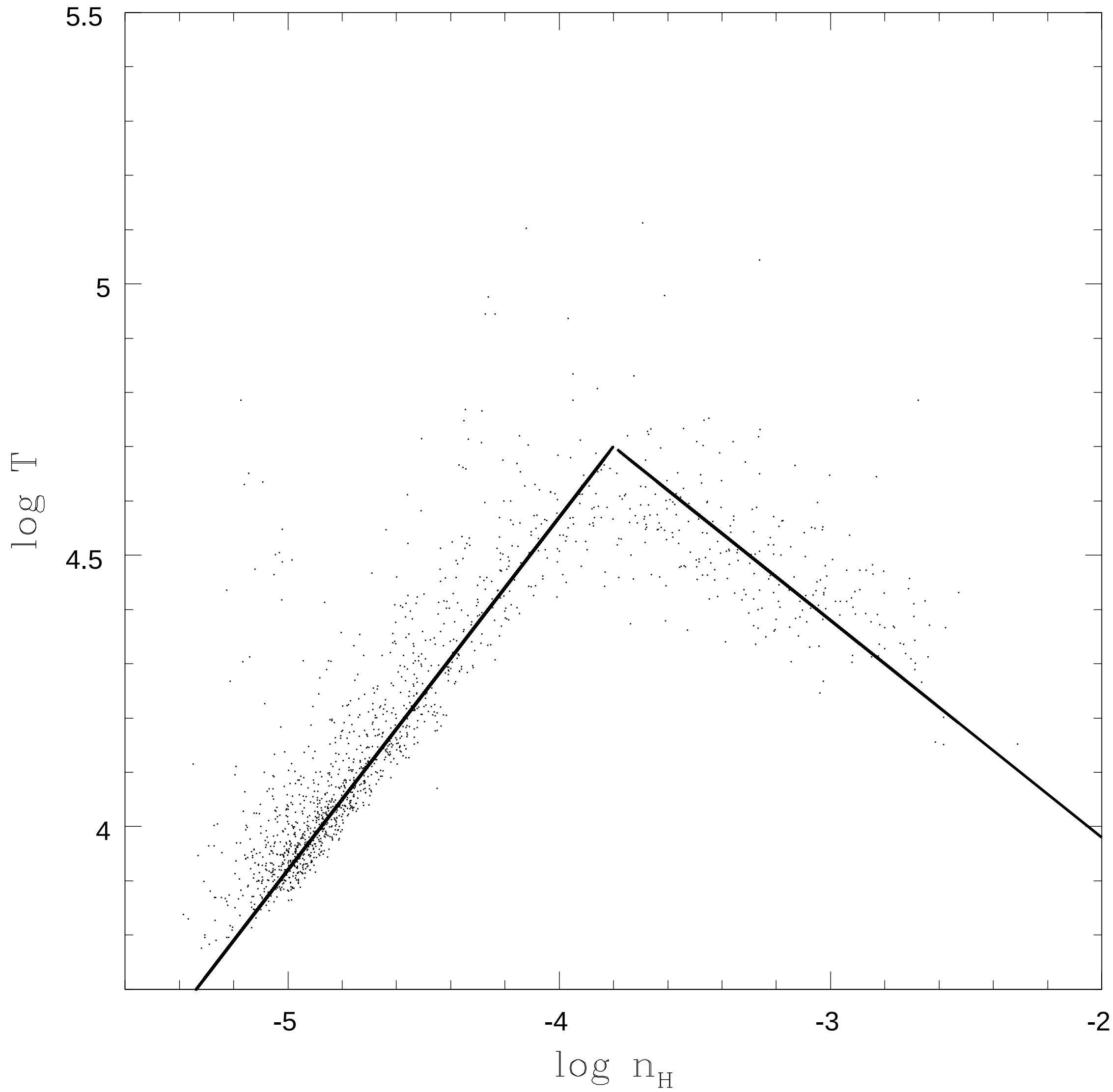

5.5
5
4.5
4
log T
-5
-4
-3
-2
log n_H

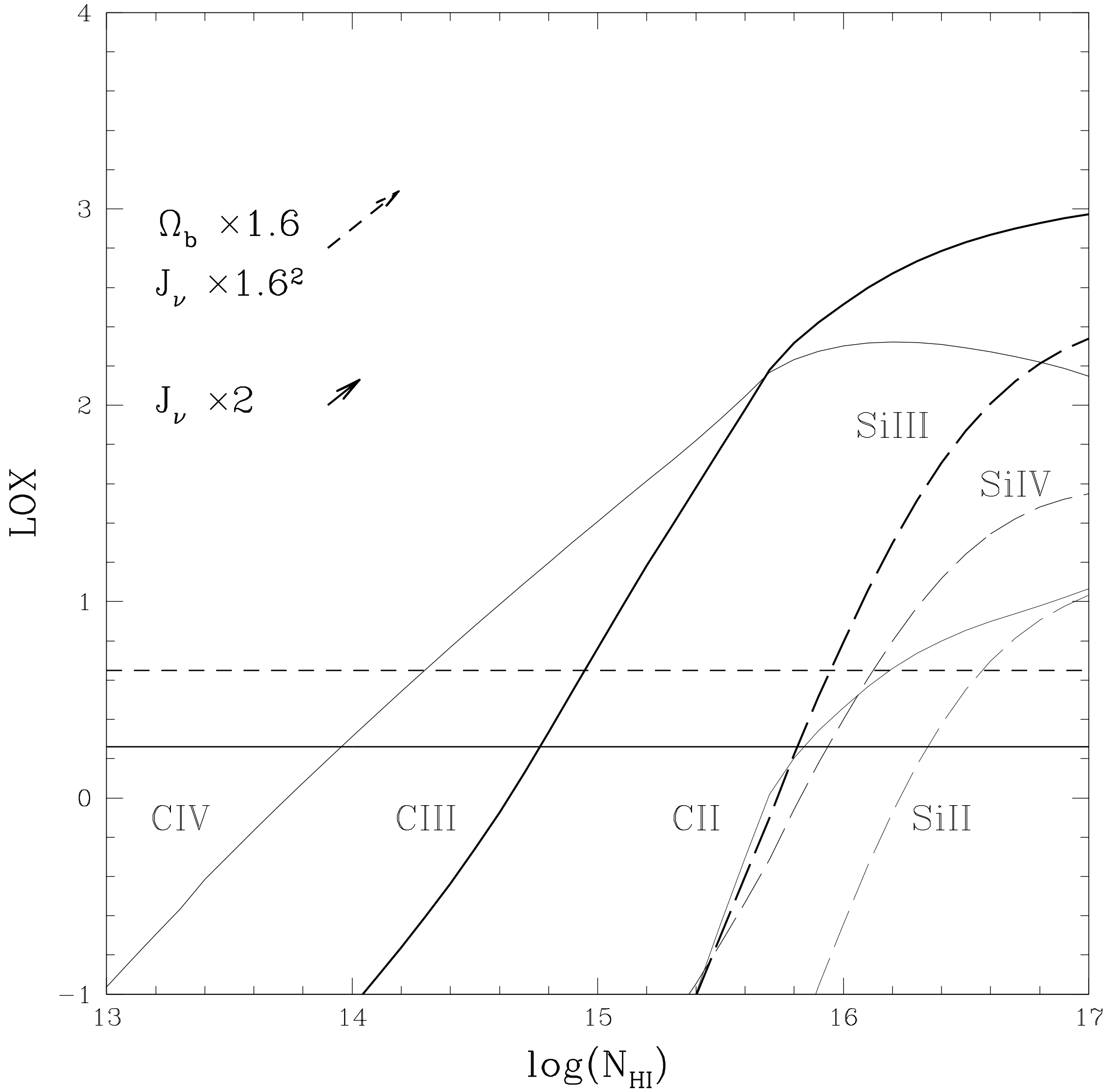

LOX
log(N_{HI})
Ω_b ×1.6
J_ν ×1.6²
J_ν ×2
SiIII
SiIV
CIV
CIII
CII
SiII

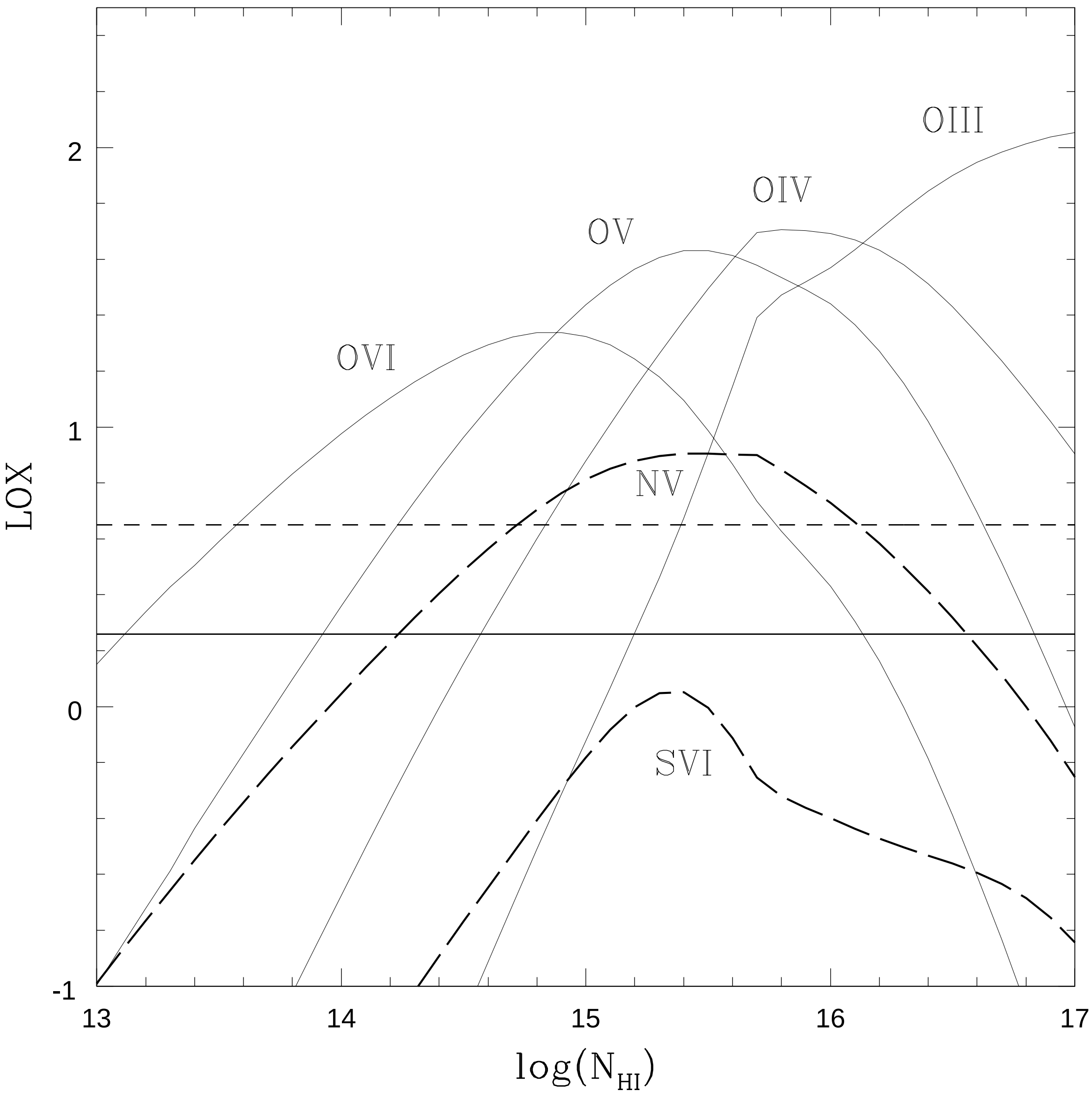

OIII
OIV
OV
OVI
NV
SVI
LOX
log(N_HI)
-1
0
1
2
13
14
15
16
17